Short communication

# Revisiting silibinin as a novobiocin-like Hsp90 C-terminal inhibitor: Computational modeling and experimental validation

Elisabet Cuyàs[a,b,1], Sara Verdura[a,b,1], Vicente Micol[c], Jorge Joven[d], Joaquim Bosch-Barrera[b,e,f], José Antonio Encinar[c,**], Javier A. Menendez[a,b,*]

[a] ProCURE (Program Against Cancer Therapeutic Resistance), Metabolism and Cancer Group, Catalan Institute of Oncology, Girona, Spain
[b] Girona Biomedical Research Institute (IDIBGI), Girona, Spain
[c] Institute of Research, Development and Innovation in Biotechnology of Elche (IDiBE), and Molecular and Cell Biology Institute (IBMC), Miguel Hernández University (UMH), Elche, Spain
[d] Unitat de Recerca Biomèdica, Hospital Universitari Sant Joan, Institut d'Investigació Sanitària Pere Virgili, Universitat Rovira i Virgili, Reus, Spain
[e] Medical Oncology, Catalan Institute of Oncology (ICO), Girona, Spain
[f] Department of Medical Sciences, Medical School University of Girona, Girona, Spain

## ARTICLE INFO

## ABSTRACT

The flavonolignan silibinin is the major component of the extract isolated from the seeds of the milk thistle (*Silybum marianum*). Herein, we performed an *in silico* analysis focusing on the molecular docking of the putative atomic interactions between silibinin and heat shock protein 90 (Hsp90), an adenosine triphosphate-dependent molecular chaperone differentially expressed in response to microenvironmental stress. Time-resolved fluorescence resonance energy transfer was employed to measure the capacity of silibinin to inhibit Hsp90 binding to other co-chaperones with enzymatic activity. Whereas silibinin is predicted to interact with several pockets in the C-terminal domain (CTD) of Hsp90α and β, its highest-ranking docked poses significantly overlap with those of novobiocin, a well-characterized Hsp90 CTD-targeting inhibitor. The net biochemical effect of silibinin was to inhibit the efficiency of Hsp90α/β CTD binding to its co-chaperone PPID/cyclophilin D in the low millimolar range, equivalent to that observed for novobiocin. The hepatotoxicant behavior of silibinin solely occurred at concentrations several thousand times higher than those of the Hsp90 N-terminal inhibitor geldanamycin. Silibinin might be viewed as a non-hepatotoxic, novobiocin-like Hsp90 inhibitor that binds the CTD to induce changes in Hsp90 conformation and alter Hsp90-co-chaperone-client interactions, thereby providing new paths to developing safe and efficacious Hsp90 inhibitors.

## 1. Introduction

Silibinin is the major bioactive component of silymarin, a flavonolignan extract obtained from the seeds of the milk thistle herb (*Silybum marianum*) (Abenavoli et al., 2018). Silibinin-containing silymarin and new formulations of silibinin have been employed over the last 40 years as anti-hepatotoxic agents and as components of nutritional supplements aimed at preventing hepatic steatosis and protecting liver from exposure to chemical and environmental toxins (Federico et al., 2017; Gazák et al., 2007 Abenavoli et al., 2018). Moreover, an ever-growing number of studies have demonstrated the capacity of silibinin to exhibit

inhibitory activity against cultured cancer cells and tumor xenografts, to enhance the efficacy of other therapeutic agents, to reduce the toxicity of cancer treatments, and to prevent and overcome the emergence of cancer drug resistance (Bosch-Barrera and Menendez, 2015; 2017). More importantly, when used orally as part of more bioavailable formulations, silibinin has recently been shown to exhibit significant clinical activity in cancer patients with advanced systemic disease (Bosch-Barrera et al., 2014, 2016; Priego et al., 2018). Indeed, responses to silibinin-based therapy were notable in the central nervous system, where several complete responses were achieved in patients with non-small cell lung cancer (NSCLC) presenting brain metastases

---

* Corresponding author. Catalan Institute of Oncology (ICO), Girona Biomedical Research Institute (IDIBGI), Edifici M2, Parc Hospitalari Martí i Julià, E-17190, Salt, Girona, Spain.
** Corresponding author. Instituto de Investigación, Desarrollo e Innovación en, Biotecnología Sanitaria de Elche (IDiBE), Av. de la Universidad, Edif. Torregaitan, Despacho 2.08, E-03202, Elche, Alicante, Spain.
E-mail addresses: jant.encinar@umh.es (J.A. Encinar), jmenendez@iconcologia.net, jmenendez@idibgi.org (J.A. Menendez).
[1] These authors contributed equally.

(Priego et al., 2018).

Investigations into the molecular mechanisms involved in the aforementioned anti-cancer activities of silibinin have repeatedly confirmed its ability to function as a natural down-modulator of signal transducer and activator of transcription (STAT3) signaling (Agarwal et al., 2007; Bosch-Barrera and Menendez, 2015, 2017; Cuyàs et al., 2016). We recently combined computational and experimental approaches to confirm that silibinin can directly bind and inhibit STAT3 at both the Src homology-2 (SH2) dimerization domain and the DNA-binding transactivation domain (DBD) (Verdura et al., 2018). Accordingly, the suppressive effects of silibinin on brain metastases can be explained by its capacity to block STAT3 signaling in a sub-population of reactive astrocytes required for the maintenance of brain metastastic lesions, even at advanced stages of colonization (Priego et al., 2018). As a flavonoid, however, silibinin is expected to interact with a variety of molecular targets (Mateen et al., 2013; Tiwari and Mishra, 2015; Jahanafrooz et al., 2018), some of which might be highly relevant to those tumor lesions occurring in the brain. One such mechanism might involve heat shock protein 90 (Hsp90), an adenosine triphosphate (ATP)-dependent molecular chaperone that is critically required for the correct localization, folding, and stability of its client proteins, many of which are well-known driver oncoproteins such as STAT3.

Previous biochemical assays revealed that the inhibitory activity of silibinin against Hsp90 is likely the result of binding to the C-terminus of the protein (Zhao et al., 2011, 2012). Also, animal models confirmed the ability of silibinin to operate as an Hsp90 inhibitor targeting the pathogenesis of Cushing disease, which is caused by corticotroph adenomas of the pituitary that overexpress Hsp90 and hypersecrete adrenocorticotropin (Riebold et al., 2015a,b; Sbiera et al., 2015; Sugiyama et al., 2015). Because most of the Hsp90 client proteins belong to multiple signaling pathways, many of them linked specifically to metastatic processes, a single Hsp90 inhibitor is expected to provide the equivalent of "multitargeted" or combinatorial therapy, thereby overriding the danger of resistance phenomena. Although several Hsp90 inhibitors have demonstrated promising preclinical and clinical results in tumors that have become resistant to molecular-targeted agents, most of them are hindered by their low capacity to cross the blood-brain barrier (BBB), limited target inhibition and toxicities (Neckers and Workman, 2012; Travers et al., 2012; Blair et al., 2014; Chatterjee and Burns, 2017). Given the clinical benefit of a well-tolerated and safe oral treatment with a silibinin-containing nutraceutical for targeting secondary brain tumors (Bosch-Barrera et al., 2016; Priego et al., 2018) and the recently predicted BBB permeability of clinically relevant formulations of silibinin (Pérez-Sánchez et al., 2019), it might be relevant to reassess the proposed capacity of silibinin to target Hsp90. In this regard, liver toxicity, a leading systemic toxicity of drugs and chemicals, is demanding human-relevant *in vitro* solutions to overcome a major drawback for the therapeutic use of Hsp90 inhibition, namely the dose-limiting hepatotoxicity elicited by conventional geldanamycin-derivate Hsp90 inhibitors containing a benzoquinone moiety (Egorin et al., 1998; Dikalov et al., 2002; Cysyk et al., 2006; Lauber et al., 2015). Indeed, the clinical translation of Hsp90 blockade has largely been hampered by serious hepatotoxicity of first- and second-generation Hsp90 inhibitors. Given the well-known hepatoprotective effects of silymarin and its major active constituent silibinin and the accompanying lack of adverse effects even at high doses (Vargas-Mendoza et al., 2014; Soleimani et al., 2019), silibinin deserves to be studied as a clinically relevant non-hepatotoxic Hsp90 C-terminal inhibitor.

Herein, we present an *in silico* analysis focusing on the molecular docking of the putative atomic interactions between silibinin and Hsp90. Time-resolved fluorescence energy transfer (TR-FRET) technology was additionally employed to measure silibinin's capacity to inhibit Hsp90 binding to other co-chaperones with enzymatic activity. Comparative studies were conducted with the amino coumarin natural product novobiocin, a well-known inhibitor of the C-terminal domain (CTD) of Hsp90 (Marcu et al., 2000a,b; Matts et al., 2011). Finally, a comparative analysis of silibinin-versus geldanamycin-induced hepatotoxicity and superoxide production was conducted in HepG2 human hepatoma cells. We now provide computational and experimental evidence to propose silibinin as a novobiocin-like Hsp90 CTD inhibitor that induces changes in Hsp90 conformation and alter Hsp90-co-chaperone-client interactions without promoting unwanted biotransformation phenomena responsible for hepatotoxicity.

## 2. Materials and methods

### 2.1. Homology modeling

To date, 286 and 15 resolved structures have been deposited in the PDB for Hsp90α (UniProt code P07900, HS90A_HUMAN) and Hsp90β (UniProt code P08238, HS90B_HUMAN) proteins, respectively. For Hsp90β, the 5FWM structure represents a closed conformation. However, structures of Hsp90β in open conformations, or Hsp90α open or closed conformations have not yet been deposited in the PDB. Therefore, three-dimensional (3D) structural models of the full-length Hsp90β in open conformations were generated by homology modeling in automated mode (Biasini et al., 2014) using the 2IOQ structure as a template. Using the same methodology, 3D models were generated for the open and closed conformations of full-length Hsp90α using 2O1U and 5ULS, respectively, as templates. A description of this methodology has been previously reported (Bello-Pérez et al., 2018).
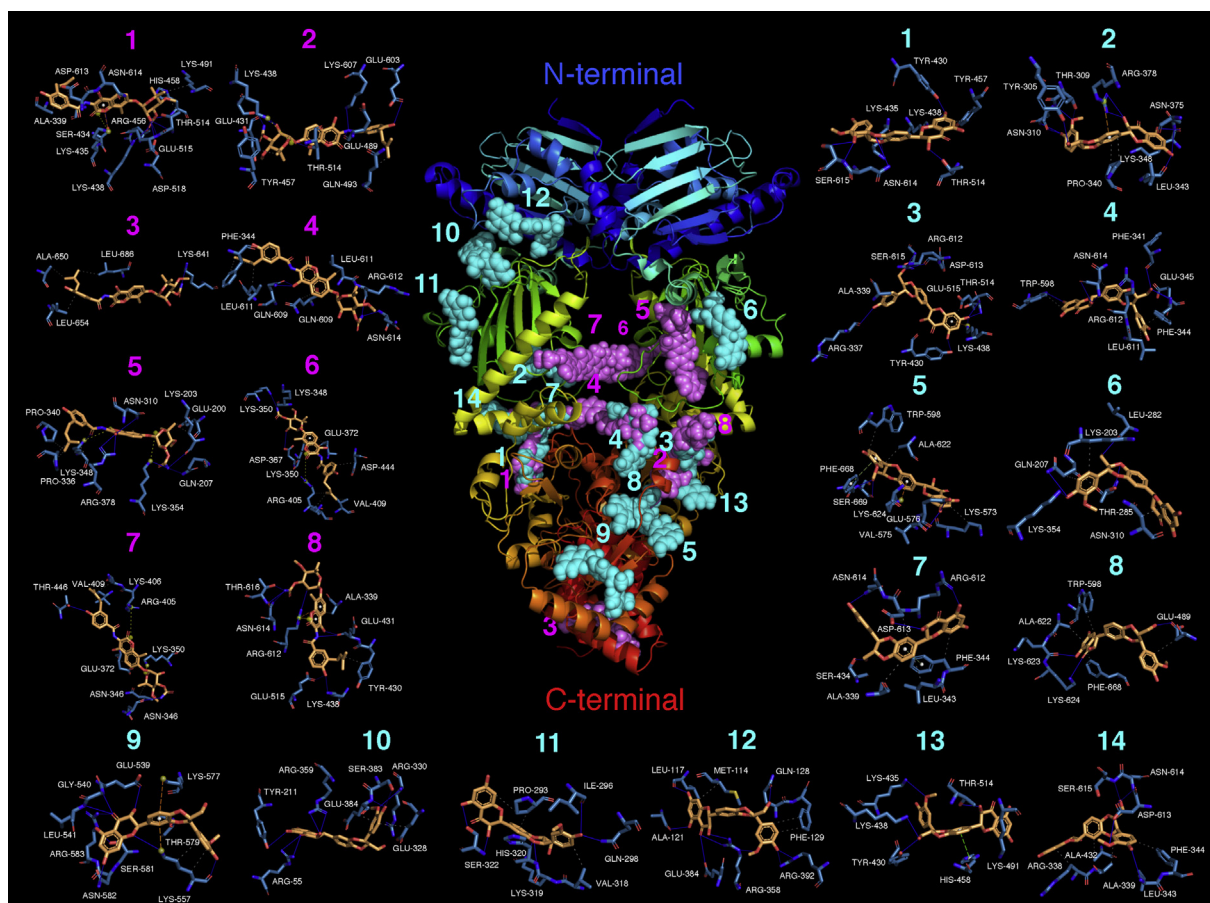
### 2.2. Molecular docking

The structures of silibinin (PubChem CID: 31553) and novobiocin (PubChem CID: 54675769) were obtained from the National Center for Biotechnology Information (NCBI) PubChem database (http://www.ncbi.nlm.nih.gov/pccompound).

Molecular docking experiments were carried out using YASARA v18.12.27 software (Krieger et al., 2004), as described (Encinar et al., 2015; Galiano et al., 2016). A total of 500 flexible docking runs were set and clustered (6 Å) around the putative binding sites, i.e., two complexed compounds belong to different clusters if the ligand Root-Mean-Square Deviation of their atomic positions is greater than a minimum of 6 Å around certain hot spot conformations. The YASARA pH command was set to 7.4. The YASARA software calculated the Gibbs free energy variation ($\Delta G$, kcal/mol), with more positive energy values indicating stronger binding. To calculate this parameter, which is used to rank compounds, Autodock Vina uses a force field scoring function that considers the strength of electrostatic interactions, hydrogen bonding between all atoms of the two binding partners in the complex, intermolecular van der Waals forces, and also solvation and entropy contributions (Lionta et al., 2014). All the values are included in the corresponding tables with a negative sign. Only the $\Delta G$ value for the best compound docked in each cluster is shown. Dissociation constants were recalculated from the average binding energy of all compounds of each cluster. The key residues of each receptor monomer (chain 1 or 2) interacting with the best ligand in each cluster were detected using also YASARA v18.12.27 software (Krieger et al., 2004). All of the figures were prepared using PyMol 2.0 software and all the interactions were detected using the PLIP algorithm (Salentin et al., 2015).

### 2.3. TR-FRET-based Hsp90 CTD activity assays

To determine the effect of novobiocin and silibinin on the activity of Hsp90, we employed TR-FRET technology using either recombinant human Hsp90α (6 ng/reaction of HSP90α [535–732] Cat. #50316, protein lot #140103-G3) or Hsp90β (6 ng/reaction of HSP90β [535–724], Cat. #50313, protein lot #130607-G) CTDs and the PPID ligand (56 nmol/L, lot# 130703), all from BPS Bioscience (San Diego, CA). The TR-FRET signal from the assay correlates with the amount of PPID ligand binding to the HSP90 CTD.

**Fig. 1. Hsp90β in a closed conformation with docked novobiocin and silibinin.** Figure depicts the backbone of the Hsp90β homodimer (PDB code 5FWM) with rainbow colors from the N-terminal (blue) to the C-terminal (red) domain. For each cluster of the docked compound (novobiocin and novobiocin cluster numbers are shown in violet while silibinin and silibinin cluster numbers are shown in cyan), only the molecule (spheres) with the best binding energy is shown. Each inset shows the detailed interactions of each compound docked to the protein, indicating the participating amino acids involved in the interaction and the type of interaction (hydrogen bonds, hydrophilic interactions, salt bridges, Π-stacking, etc). (For interpretation of the references to color in this figure legend, the reader is referred to the Web version of this article.)

The compounds were diluted in 10% DMSO and 2 μL of the dilution was added to a 20 μL reaction so that the final concentration of DMSO was 1% in all of the reactions. All binding reactions were conducted at room temperature. The 20 μL reaction mixture in C-terminal assay buffer contained the Hsp90α/β CTD, the indicated amount of the inhibitor, PPID, and the reaction dyes. The reaction mixture was incubated for 120 min prior to reading the TR-FRET signal. For the negative control, buffer was added instead of PPID. Fluorescence signals for both the donor and acceptor dyes were measured using a Tecan Infinite M1000 plate reader (Männedorf, Switzerland). TR-FRET was recorded as the ratio of the fluorescence of the acceptor and the donor dyes (acceptor/donor).

Binding experiments were performed in duplicate at each concentration. The TR-FRET data were analyzed using Graphpad Prism computer software. In wells containing PPID and no compound, the TR-FRET signal ($F_t$) in each data set was defined as 100% activity. In wells without peptide ligand, the TR-FRET signal ($F_b$) in each data set was defined as 0% activity. The percentage activity in the presence of each compound was calculated according to the following equation: % activity = $[(F-F_b)/(F_t - F_b)] \times 100$, where F = the TR-FRET signal in the presence of the compound. The percentage inhibition was calculated according to the following equation: % inhibition = 100 - % activity. To calculate the $IC_{50}$ values, the % activity versus a series of compound concentrations were plotted using non-linear regression analysis of sigmoidal dose-response generated with the equation Y = B + (T-B)/ 1 + 10∧((LogIC50-Z) × HillSlope), where Y = percent activity,

B = minimum percent activity, T = maximum percent activity, Z = logarithm of compound concentration and Hill Slope = slope factor or Hill coefficient. The $IC_{50}$ values were then determined as the concentration causing a half-maximal percent activity.

### 2.4. Reagents

Silibinin and novobiocin were purchased from Sigma-Aldrich (St. Louis, MO). Geldanamycin and ganetespib (STA-9090) were purchased from Selleckchem.com. All reagents were dissolved in dimethylsulfoxide (DMSO) to prepare 10 mmol/L stock solutions, which were stored at −80 °C until use.

### 2.5. Metabolic status assessment

Cell viability was determined using standard colorimetric MTT-based reduction assays.

### 2.6. Mitochondrial ROS measurements

To detect mitochondrial ROS, HepG2 liver cancer cells (a kind gift from Dr. Jose Manuel Fernández-Real, Girona, Spain) were treated with rotenone, geldanamycin, ganetespib (STA-909), novobiocin or silibinin for 18 h and then incubated at 37 °C with MitoSOX (5 μM; Invitrogen) for 20 min in PBS, washed three times with PBS and analyzed by flow cytometry.

## 2.7. Statistical analysis

All statistical analyses were performed using XLSTAT 2010 (Addinsoft™). Data are presented as mean ± S.D. Comparisons of means of ≥3 groups were performed by ANOVA, and the existence of individual differences, in case of significant $F$ values at ANOVA, were tested by Scheffé's multiple contrasts. $P$ values < 0.05 were considered to be statistically significant (denoted as *). All statistical tests were two-sided.

## 3. Results

Molecular docking assays of silibinin and novobiocin against Hsp90α and β isoforms, which are differently expressed in embryonic and adult tissues and exhibit significantly different behaviors with respect to substrate/client interactions under stress conditions (Taherian et al., 2008), were performed as previously described (Encinar et al., 2015; Galiano et al., 2016). The selected protein structures, either from the Protein Data Bank (PDB) or homology modeled, were subjected to geometry optimization using the repair function of the FoldX algorithm (Schymkowitz et al., 2005). To search for potential binding sites of silibinin and novobiocin, a global molecular docking procedure was performed with AutoDock Vina using YASARA software (Krieger and Vriend, 2014), where a total of 500 flexible docking runs were set and clustered around the putative binding sites.

### 3.1. Prediction of the Hsp90β-silibinin interactions

Docking simulations of novobiocin and silibinin in the closed conformation of Hsp90β (5FWM structure) produced eight and fourteen clusters of docking poses, respectively (Fig. 1). The docking results were ranked according to the ascent of the binding energies for novobiocin (up to −10.124 kcal/mol) and silibinin (up to −9.408 kcal/mol) (Table 1). A careful inspection of the different conformations showed that, in the #1 ranked cluster of both compounds, the Hsp90β-silibinin interaction shared approximately 80% of the twenty-four participating amino acid residues involved in the novobiocin binding mode to the chain 1 of closed Hsp90β (ALA339, PRO340, PHE341, LEU343, TYR430, GLU431, ALA432, SER434, LYS435, LYS438, ARG456, TYR457, HIS458, LYS491, TYR512, MET513, THR514, and GLY515; Table 1), and 100% of the three amino acid residues involved in the novobiocin binding mode to the chain 2 ASP613, ASN614, SER615; Table 1).

Upon generation of a computational homology model (Biasini et al., 2014) of Hsp90β in its open conformation (Dollins et al., 2007), docking simulations of novobiocin and silibinin similarly produced four clusters of docking poses for each compound (Fig. 2), with binding energies up to −9.41 kcal/mol for novobiocin and −8.789 kcal/mol for silibinin. The binding mode of silibinin in the #1 ranked cluster shared 50% of the twenty participating amino acid residues involved in the novobiocin binding mode to the chain 1 of closed Hsp90β (ASN30, TYR33, ILE38, ARG41, HIS205, GLU303, LYS306, TRP312, ASP314, and ARG337; Table 2).

### 3.2. Prediction of the Hsp90α-silibinin interactions

Docking simulations of novobiocin and silibinin in a homology model of the closed conformation of Hsp90α produced three and eight clusters of docking poses, respectively (Fig. 3). Binding energies were −9.043 kcal/mol for novobiocin and −9.703 kcal/mol for silibinin in the #1 ranked cluster; the binding mode of the docked silibinin was similar to the binding observed for novobiocin in the #2 ranked cluster, in which silibinin shared approximately 40% of the twenty-one participating amino acid residues involved in the novobiocin binding mode to the chain 1 of closed Hsp90α (ASN354, LYS356, LYS357, LYS358, GLU374, ASN383, LEU447, and GLU451), and 25% of the four amino acid residues involved in the novobiocin binding mode to the chain 2 (LEU619) (Table 3).

Upon generation of a computational homology model of Hsp90α in its open conformation, docking simulations of novobiocin and silibinin produced four and three clusters of docking poses, respectively (Fig. 4). Binding energies were −9.742 kcal/mol for novobiocin and −10.344 kcal/mol for silibinin in the #1 ranked cluster. The binding mode of silibinin in such cluster shared an approximately 52% of the twenty-seven amino acid residues involved in the novobiocin binding mode to the chain 1 of open Hsp90α (SER50, SER53, ASP54, ASP57, GLN212, PHE213, ILE214, GLY215, TRP297, PHE312, SER315, LEU316, LYS362, and TYR364; Table 4).

### 3.3. Silibinin inhibits Hsp90α/β activity

We investigated the inhibitory effect of silibinin and novobiocin on Hsp90 activity using time-resolved fluorescence resonance energy transfer (TR-FRET) assays, which were designed to measure the inhibition of the Hsp90α/β CTD binding to its protein target PPID/cyclophilin D. The assay samples contained terbium-labeled donor, dye-labeled acceptor, Hsp90α/β CTD, GST-tagged PPID and silibinin/novobiocin, and were incubated for 2 h. The Hsp90α/β CTD-PPID interaction was then assayed by measuring the TR-FRET signal using a fluorescence reader.

The addition of increasing concentrations of silibinin decreased the TR-FRET signal in a dose-dependent manner (Fig. 5A), suggesting that it inhibited the interaction between Hsp90α/β and PPID. The IC$_{50}$ was 1 mmol/L when employing Hsp90α CTD and 2 mmol/L when using Hsp90β CTD. We also tested in parallel the effect of novobiocin in the TR-FRET competition assay. As expected, novobiocin dose-dependently decreased the TR-FRET signal with an IC$_{50}$ of ∼0.5 mmol/L (Fig. 5B).

### 3.4. Silibinin is less hepatotoxic than the Hsp90 N-terminal inhibitor geldanamycin

We next analyzed the hepatic tolerability of silibinin by the human liver cell line HepG2, which has been used to classify chemical entities for hepatotoxicity and proposed as a non-animal alternative for systemic toxicology (Van den Hof et al., 2014; Ramirez et al., 2018). When cellular viability was examined by MTT-based assays, HepG2 were markedly less susceptible toward silibinin and novobiocin as reflected by half-maximal cell viability inhibitory concentrations (IC$_{50}$) thousand of times beyond the IC$_{50}$ values obtained with the Hsp90 N-terminal domain inhibitors geldanamycin and ganetespib (Wang et al., 2010; Shimamura et al., 2012) (Fig. 6A).

Mitochondrial O$_2^-$ was then quantified with MitoSOX-Red staining in HepG2 cells (Fig. 6B). MitoSOX-reactive mitochondrial ROS levels were increased following exposure of HepG2 cells to rotenone, a mitochondrial respiratory complex I that has been shown to produce O$_2^-$ (Shimura et al., 2017), in response to the Hsp90 inhibitor geldanamycin, which is known to promote superoxide formation by enzymatic and non-enzymatic redox cycling (Dikalov et al., 2002), but not in response to either the resorcionol-triazole Hsp90 inhibitor ganetespib, which lacks the benzoquinone moiety of geldanamycin (Jhaveri and Modi, 2015), or the Hsp90 CTD inhibitor novobiocin. Silibinin was the sole Hsp90 inhibitor tested capable of decreasing O$_2^-$ levels in HepG2 cells compared with non-treated control cells (Fig. 6B).

## 4. Discussion

Hsp90 is important in maintaining the structural integrity of over 200 client proteins including many well-known signal transducers, some of which may have beneficial effects for metastasis-initiating cells. Indeed, Hsp90 is the most highly expressed cellular protein involved in the stabilization and degradation of other proteins under biophysical stress conditions such as those normally found in the harsh tumor

**Table 1**
Interactions between novobiocin/silibinin and the closed conformation of the Hsp90β dimer.

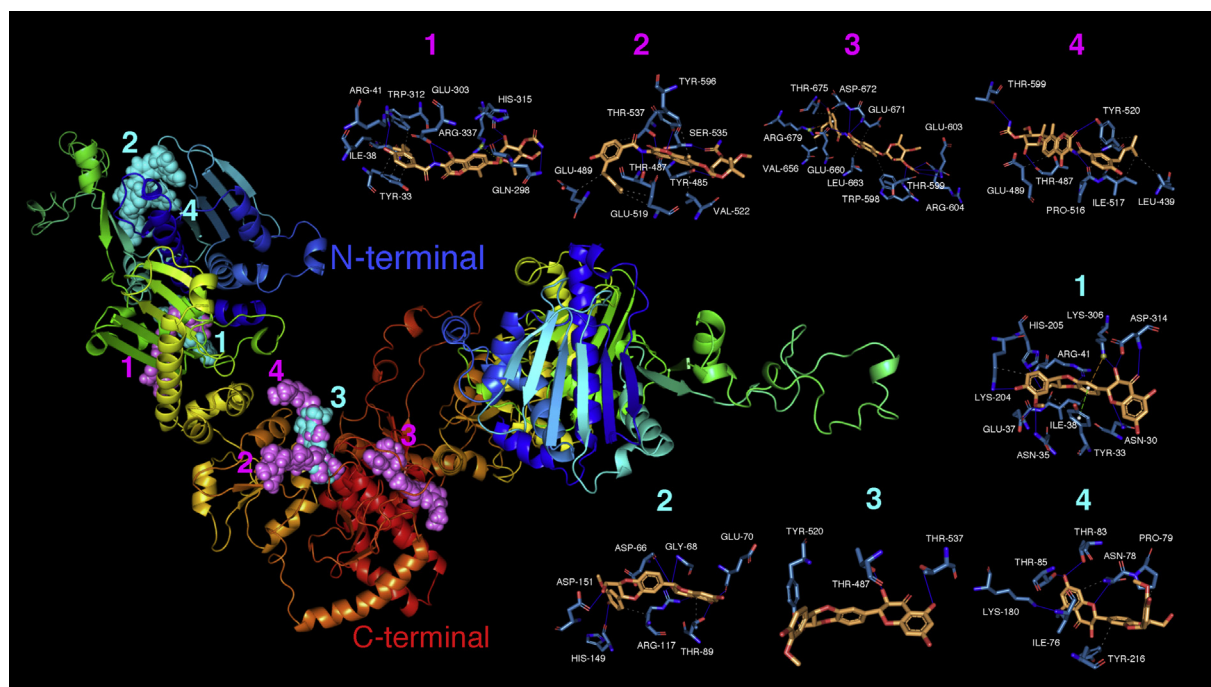| Cluster number | ΔG, [kcal/mol] | Dissoc. constant, [μM] | Participating amino acids interacting with novobiocin |
|---|---|---|---|
| 1 | −10.124 | 0.037932336 | ARG337, ARG338, ALA339, PRO340, PHE341, LEU343, PHE344, TYR430, GLU431, ALA432, SER434, LYS435, LYS438, ARG456, TYR457, HIS458, MET466, SER490, LYS491, TYR512, MET513, THR514, GLU515, ASP518 (**chain 1**) and ASP613, ASN614, SER615 (**chain 2**) |
| 2 | −9.15 | 0.196318422 | GLU603, LYS607, ASP613, TYR619, SER669, LEU670, GLU671, ASP672, PRO673 (**chain 1**) and TYR430, GLU431, SER434, LYS438, ARG456, TYR457, HIS458, MET466, GLU489, SER490, LYS491, GLN493, TYR512, MET513, THR514, GLU515, PRO516 (**chain 2**) |
| 3 | −8.977 | 0.262888594 | LEU638, LYS641, ASP648, ALA650, VAL651, ASP653, LEU654, MET683, ILE684, LEU686, GLY687, LEU688 (**chain 1**) and ALA650, VAL651, ASP653, LEU654, LEU657, ARG682, MET683, ILE684, LEU686, GLY687, LEU688 (**chain 2**) |
| 4 | −8.918 | 0.290415188 | PHE341, PHE344, GLU345, GLN609, ALA610, LEU611, ARG612, ASN614, MET617 (**chain, 1**) and PHE341, ASP342, PHE344, GLU345, GLN609, LEU611, ARG612, ASP613, THR616 (**chain 2**) |
| 5 | −8.875 | 0.312276094 | GLU200 LYS203 LYS204 GLN207 TYR305 LEU308 THR309 ASN310 ASP311 PRO336 ARG338 ALA339 PRO340 PHE341 LYS348 LYS349 ASN351 LYS354 PHE361 ASP364 PHE376 ARG378 PHE433 (**chain 1**) |
| 6 | −8.832 | 0.335782594 | ASN346 LYS347 LYS348 LYS349 LYS350 (**chain 1**) and ASN346 LYS350 ASP367 PRO371 GLU372 TYR373 ARG405 LYS406 VAL409 LYS410 GLU443 ASP444 SER445 THR446 ASN447 (**chain 2**) |
| 7 | −8.769 | 0.373454563 | ASN346 LYS347 LYS350 ASP367 PRO371 GLU372 ARG405 LYS406 VAL409 LYS410 GLU443 ASP444 SER445 THR446 ASN447 (**chain 1**) and ASN346 LYS347 LYS348 LYS350 (**chain 2**) |
| 8 | −8.748 | 0.386928719 | ARG612 ASP613 ASN614 SER615 THR616 MET617 (**chain 1**) and ARG338 ALA339 PHE341 TYR430 GLU431 ALA432 PHE433 SER434 LYS435 LYS438 ARG456 HIS458 MET466 THR514 GLU515 (**chain 2**) |

| Cluster number | ΔG, [kcal/mol] | Dissoc. constant, [μM] | Participating amino acids interacting with silibinin |
|---|---|---|---|
| 1 | −9.408 | 0.127011 | ALA339, PRO340, PHE341, LEU343, PHE344, TYR430, GLU431, ALA432, PHE433, SER434, LYS435, LYS438, ARG456, TYR457, HIS458, LYS491, TYR512, MET513, THR514, GLU515 (**chain 1**) and ARG612, ASP613, ASN614, SER615 (**chain 2**) |
| 2 | −9.256 | 0.164158 | TYR305, THR309, ASN310, ASP311, PRO336, ARG338, PRO340, ASP342, LEU343, PHE344, GLU345, ASN346, LYS348, LYS349, LYS350, ASN351, ASN352, ASN375, PHE376, ARG378 (**chain 1**) |
| 3 | −9.094 | 0.215779 | ARG612, ASP613, ASN614, SER615, THR616 (**chain 1**) and ARG337, ARG338, ALA339, TYR430, GLU431, ALA432, SER434, LYS438, ARG456, TYR457, MET513, THR514, GLU515, ASP518 (**chain 2**) |
| 4 | −9.087 | 0.218343 | TRP598, MET602, MET606, LYS607, ALA610, LEU611, ARG612, ASP613, ASN614, MET617, MET621 (**chain 1**) and PHE341, ASP342, LEU343, PHE344, GLU345, ASN346 (**chain 2**) |
| 5 | −8.873 | 0.313332 | LYS573, LYS574, VAL575, GLU576, ILE591, VAL592, THR593, TRP598, THR599, ALA600, MET602, GLU603, ALA622, LYS623, LYS624, HIS625, PHE668, SER669 (**chain 1**) |
| 6 | −8.802 | 0.353222 | VAL202, LYS203, GLN207, PHE208, GLU281, LEU282, ASN283, LYS284, THR285, PHE304, LYS306, SER307, LEU308, ASN310, ASP311, TRP312, LYS354, TYR356 (**chain 1**) |
| 7 | −8.632 | 0.470608 | ALA339, PRO340, PHE341, ASP342, LEU343, PHE344, GLU345, GLU431, ALA432, PHE433, SER434, LYS435, GLU515 (**chain 1**) and LEU611, ARG612, ASP613, ASN614, THR616 (**chain 2**) |
| 8 | −8.596 | 0.500090 | THR593, TRP598, THR599, MET602, GLU603, LYS607, GLY618, TYR619, ALA622, LYS623, LYS624, PHE668, SER669, LEU670, GLU671, ASP672, PRO673 (**chain 1**) and GLU489, SER490, GLN493 (**chain 2**) |
| 9 | −8.561 | 0.530522 | GLU539, GLY540, LEU541, LEU543, GLU545, LYS550, MET553, LYS557, ALA558, GLU561, CYS564, LYS565, LYS577, THR579, ILE580, SER581, ASN582, ARG583, GLU627 (**chain 1**) |
| 10 | −8.452 | 0.637678 | ASP52, ARG55, ASP122, SER124, GLY210, TYR211, TRP289, THR290, GLU328, PHE329, ARG330, ARG359, ASP382, SER383, GLU384, ASP385 (**chain 1**) |
| 11 | −8.425 | 0.667410 | ILE288, ASN292, PRO293, ASP294, ILE296, GLN298, TYR301, VAL318, LYS319, HIS320, PHE321, SER322, GLU324, LEU332, GLU418 (**chain 1**) |
| 12 | −8.415 | 0.678770 | PHE113, MET114, LEU117, GLN118, GLY120, ALA121, ASP122, ILE123, SER124, GLY127, GLN128, PHE129, VAL357, ARG358, GLU384, ASP385, LEU386, LEU388, ARG392 (**chain 1**) |
| 13 | −8.400 | 0.696174 | ASP613 (**chain 1**) and TYR430, GLU431, SER434, LYS435, LYS438, ARG456, TYR457, HIS458, ASP464, SER490, LYS491, TYR512, MET513, THR514, GLU515 (**chain 2**) |
| 14 | −8.354 | 0.752379 | GLU313, ARG337, ARG338, ALA339, PRO340, PHE341, LEU343, PHE344, LYS428, GLU431, ALA432, LYS435 (**chain 1**) and LEU611, ARG612, ASP613, ASN614, SER615 (**chain 2**) |

microenvironment (Barrott and Haystead, 2013). Not surprisingly, Hsp90 inhibition has received special attention for therapeutic applications and, currently, more than twenty Hsp90-targeting drugs have entered clinical trials, with many more compounds in preclinical development (Neckers and Workman, 2012; Travers et al., 2012; Blair et al., 2014; Chatterjee and Burns, 2017). Here, we provide computational and experimental evidence confirming and extending previous studies suggesting that Hsp90 is a primary target of silibinin.

Although it should be acknowledged that Hsp90 inhibitors have shown limited efficacy as single agents in a majority of cancer patients, a particularly relevant exception to this is NSCLC harboring *ALK* gene rearrangements, a genotypically-defined NSCLC subtype in which the brain is frequently a site of disease progression (Gallegos Ruiz et al., 2008; Sequist et al., 2010; Socinski et al., 2013; Zhang et al., 2015). Inhibition of Hsp90 with drugs such as ganetespib, AUY922, retispamycin, and IPI-504 leads to degradation of the oncogenic ALK fusion protein and tumor regression, even in NSCLC with acquired resistance to ALK tyrosine kinase inhibitors. We show here that silibinin,

whose administration in NSCLC patients with brain metastasis reduces lesions in the absence of adverse effects (Bosch-Barrera et al., 2016; Priego et al., 2018), is a novobiocin-like Hsp90 inhibitor that binds to a putative ATP site at the CTD of Hsp90. Of note, novobiocin used at high concentrations has been suggested to directly target the N-terminal ATP binding pocket of Hsp90 in addition to the more sensitive CTD binding site, which might be involved in the shared effects of novobiocin and silibinin. In this regard, structure activity relationship studies have identified some of the key structural features required for the scaffold cytotoxic activity of silibinin, in which Hsp90 inhibition could play a part (Zhao et al., 2011).

Refolding assays employing thermally denatured firefly luciferase, a sensitive model substrate to study folding and renaturation of denatured proteins after heat stress (Thulasiraman and Matts, 1996), revealed that silibinin could inhibit Hsp90-dependent refolding of luciferase in rabbit reticulocyte lysates by approximately 50%, at a concentration of 250 μmol/L (Zhao et al., 2011). Subsequent studies revealed the capacity of silibinin to induce a concentration-dependent
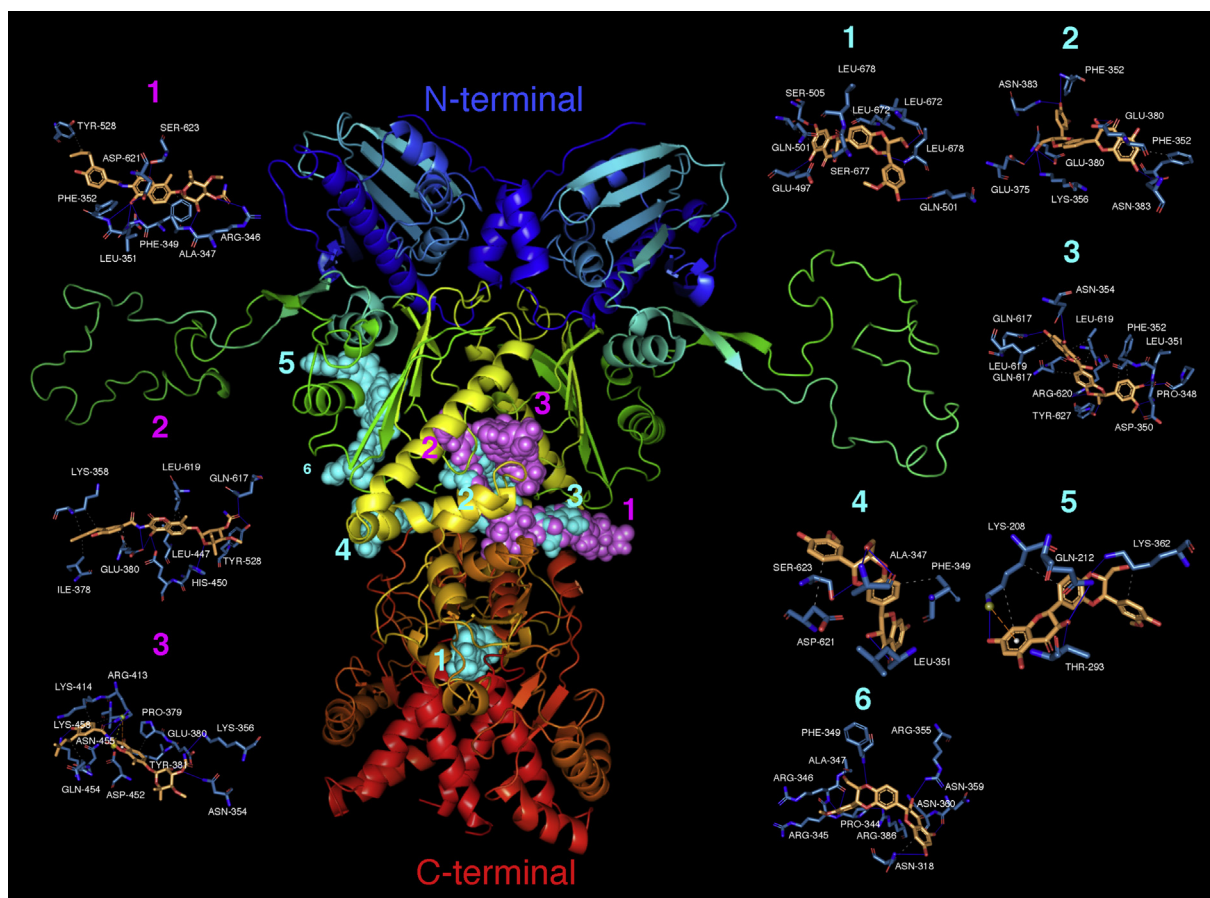
**Fig. 2. Hsp90β in an open conformation with docked novobiocin and silibinin.** Figure depicts the backbone of the Hsp90β homodimer generated by homology modeling with rainbow colors from the N-terminal (blue) to the C-terminal (red) domain. For each cluster of the docked compound (novobiocin and novobiocin cluster numbers are shown in violet while silibinin and silibinin cluster numbers are shown in cyan), only the molecule (spheres) with the best binding energy is shown. Each inset shows the detailed interactions of each compound docked to the protein, indicating the participating amino acids involved in the interaction and the type of interaction (hydrogen bonds, hydrophilic interactions, salt bridges, Π-stacking, etc). Note: For simplicity, the figure only displays the clusters in one of the subunits. (For interpretation of the references to color in this figure legend, the reader is referred to the Web version of this article.)

degradation of several Hsp90-dependent client proteins (e.g., HER2, Raf-1 and Akt) without affecting Hsp90 protein levels. Hsp90 plays an obligatory role for the heme-regulated eukaryotic initiation factor 2 alpha kinase (HRI) to acquire and maintain an activatable conformation (Uma et al., 1997). When assessing the ability of silibinin to inhibit Hsp90-dependent activation of HRI (Shao et al., 2001, 2003; Yun et al., 2004a,b), it was found to inhibit the Hsp90-dependent maturation and activation of newly synthesized HRI in a heme-deficient lysate in a dose-dependent manner (Zhao et al., 2011). Because it failed to disrupt the interactions between Hsp90 and the co-chaperone Cdc37 with HRI,

silibinin was suggested to inhibit Hsp90 in a manner similar to that proposed for the prenylated isoflavone derrubone (Hadden et al., 2007; Hastings et al., 2008; Mays et al., 2010). Given their pharmacological similarity, subsequent studies suggested that silibinin should operate analogously to novobiocin, an amino coumarin that induces concentration-dependent degradation of Hsp90 client proteins by interacting with a previously unrecognized ATP-binding domain in the CTD of Hsp90 (Marcu et al., 2000a,b; Matts et al., 2011). When employing a refined binding assay in which silibinin was immobilized and recombinant Hsp90α CTD was allowed to bind (Young et al., 2003),

**Table 2**
Interactions between novobiocin/silibinin and the open conformation of the Hsp90β dimer.

| Cluster number | ΔG, [kcal/mol] | Dissoc. constant, [μM] | Participating amino acids interacting with novobiocin |
|---|---|---|---|
| 1 | −9.41 | 0.126583 | ASN30, TYR33, ILE38, ARG41, HIS205, GLN298, GLU299, GLY302, GLU303, LYS306, TRP312, ASP314, HIS315, LEU316, ALA317, VAL318, ARG337, LEU419, ASP422, ASN425 (**chain 1**) |
| 2 | −9.186 | 0.184745 | TYR485, THR487, GLY488, GLU489, GLN493, PHE499, GLU519, VAL522, GLN523, LYS526, LEU533, VAL534, SER535, THR537, TYR596, ASN601, PHE668 (**chain 1**) and GLN674 (**chain 2**) |
| 3 | −8.739 | 0.392851 | LYS574, GLY597, TRP598, THR599, ALA600, GLU603, ARG604, ILE605, ALA622, LYS652, VAL656, PHE659, GLU660, LEU663, GLY667, SER669, LEU670, GLU671, ASP672, THR675, ARG679 (**chain 1**) and GLU492, ASN496 (**chain 2**) |
| 4 | −8.505 | 0.583112 | LEU439, THR487, GLY488, GLU489, PRO516, ILE517, GLU519, TYR520, THR537, TYR596, THR599, ALA600, ASN601, SER666 (**chain 1**) |

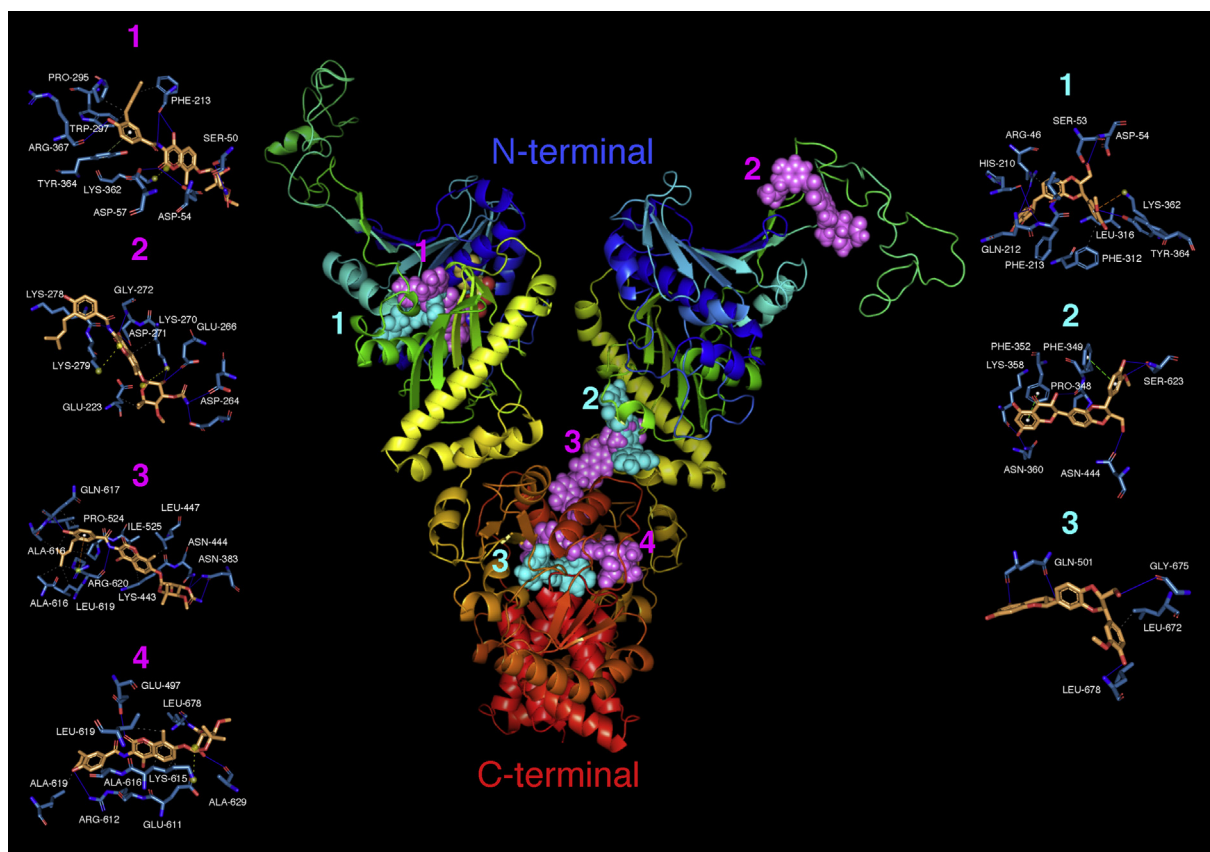| Cluster number | ΔG, [kcal/mol] | Dissoc. constant, [μM] | Participating amino acids interacting with silibinin |
|---|---|---|---|
| 1 | −8.789 | 0.361058 | ASN30, TYR33, ASN35, GLU37, ILE38, ARG41, LYS204, HIS205, GLU303, LYS306, TRP312, GLU313, ASP314, ARG337 (**chain 1**) |
| 2 | −8.459 | 0.630188 | LEU65 ASP66 SER67 GLY68 GLU70 LEU71 LYS72 THR89 LYS148 HIS149 ASN150 ASP151 ILE175 GLY176 ARG177 (**chain 1**) |
| 3 | −8.178 | 0.101262 | THR487, GLY488, GLU489, PHE499, THR514, GLU515, PRO516, GLU519, TYR520, THR537, TYR596, ALA600, ASN601, SER665, SER666, PHE668 (**chain 1**) and GLN674 (**chain 2**) |
| 4 | −7.819 | 0.1856081 | ILE76 PRO77 ASN78 PRO79 GLU81 THR83 THR85 LYS180 ILE182 LEU193 GLU194 GLU195 TYR216 GLU218 LYS266 (**chain 1**) |

**Fig. 3. Hsp90α in a closed conformation with docked novobiocin and silibinin.** Figure depicts the backbone of the Hsp90α homodimer generated by homology modeling with rainbow colors from the N-terminal (blue) to the C-terminal (red) domain. For each cluster of the docked compound (novobiocin and novobiocin cluster numbers are shown in violet while silibinin and silibinin cluster numbers are shown in cyan), only the molecule (spheres) with the best binding energy is shown. Each inset shows the detailed interactions of each compound docked to the protein, indicating the participating amino acids involved in the interaction and the type of interaction (hydrogen bonds, hydrophilic interactions, salt bridges, Π-stacking, etc). (For interpretation of the references to color in this figure legend, the reader is referred to the Web version of this article.)

**Table 3**
Interactions between novobiocin/silibinin and the closed conformation of the Hsp90α dimer.

| Cluster number | ΔG, [kcal/mol] | Dissoc. constant, [μM] | Participating amino acids interacting with novobiocin |
|---|---|---|---|
| 1 | −9.043 | 0.235176 | TYR528, MET614, GLN617, LEU619, ARG620, ASP621, ASN622, SER623, TYR627 (**chain 1**) and ARG346, ALA347, PRO348, PHE349, ASP350, LEU351, PHE352, GLU353, GLU439, GLN440 (**chain 2**) |
| 2 | −8.826 | 0.339200 | ASN354, LYS356, LYS357, LYS358, ASN360, ASP372, CYS374, GLU375, ILE378, PRO379, GLU380, LEU382, ASN383, LEU447, HIS450, GLU451, ILE525, TYR528, ILE613, MET614, GLN617 (**chain 1**) and LYS356, ALA616, ALA618, LEU619 (**chain 2**) |
| 3 | −8.624 | 0.477006 | PRO379, GLU380, TYR381, ARG413, LYS414, VAL417, LYS418, HIS450, GLU451, ASP452, GLN454, ASN455, LYS458 (**chain 1**) and GLU353, ASN354, LYS356 (**chain 2**) |

| Cluster number | ΔG, [kcal/mol] | Dissoc. constant, [μM] | Participating amino acids interacting with silibinin |
|---|---|---|---|
| 1 | −9.703 | 0.077198 | THR495, GLY496, GLU497, GLN501, VAL502, SER505, ASN609, ARG612, LEU672, SER673, SER674, GLY675, PHE676, SER677, LEU678, PRO681 (**chain 1**) and GLU497, GLN501, ARG612, LEU672, SER673, SER674, GLY675, PHE676, SER677, LEU678, PRO681 (**chain 2**) |
| 2 | −8.914 | 0.292382 | PHE352, ASN354, ARG355, LYS356, LYS357, LYS358, GLU375, GLU380, TYR381, ASN383, LEU447, GLU451, LEU619 (**chain 1**) and LEU351, PHE352, ASN354, ARG355, LYS356, LYS358, GLU380, ASN383, LEU447, LEU619 (**chain 2**) |
| 3 | −8.557 | 0.534116 | ASN354, GLN617, LEU619, ARG620, ASP621, SER623, TYR627 (**chain 1**) and PRO348, PHE349, ASP350, LEU351, PHE352, GLU353, GLN617, LEU619 (**chain 2**) |
| 4 | −8.246 | 0.902821 | ARG346, ALA347, PHE349, LEU351, PHE352, GLU353, GLU439, GLN440 (**chain 1**) and LEU619, ARG620, ASP621, ASN622, SER623 (**chain 2**) |
| 5 | −8.187 | 0.997354 | LYS208, LYS209, GLN212, LYS292, THR293, SER315, LEU316, THR317, ASN318, ASN359, ASN360, LYS362, ASP372, ARG386, GLY387 (**chain 1**) |
| 6 | −8.085 | 1.184721 | TYR313, THR317, ASN318, ASP319, GLU321, PRO344, ARG345, ARG346, ALA347, PRO348, PHE349, ASP350, ARG355, ASN359, ASN360, LYS362, ARG386 (**chain 1**) |

**Fig. 4. Hsp90α in an open conformation with docked novobiocin and silibinin.** Figure depicts the backbone of the Hsp90α homodimer generated by homology modeling with rainbow colors from the N-terminal (blue) to the C-terminal (red) domain. For each cluster of the docked compound (novobiocin and novobiocin cluster numbers are shown in violet while silibinin and silibinin cluster numbers are shown in cyan), only the molecule (spheres) with the best binding energy is shown. Each inset shows the detailed interactions of each compound docked to the protein, indicating the participating amino acids involved in the interaction and the type of interaction (hydrogen bonds, hydrophilic interactions, salt bridges, Π-stacking, etc). (For interpretation of the references to color in this figure legend, the reader is referred to the Web version of this article.)
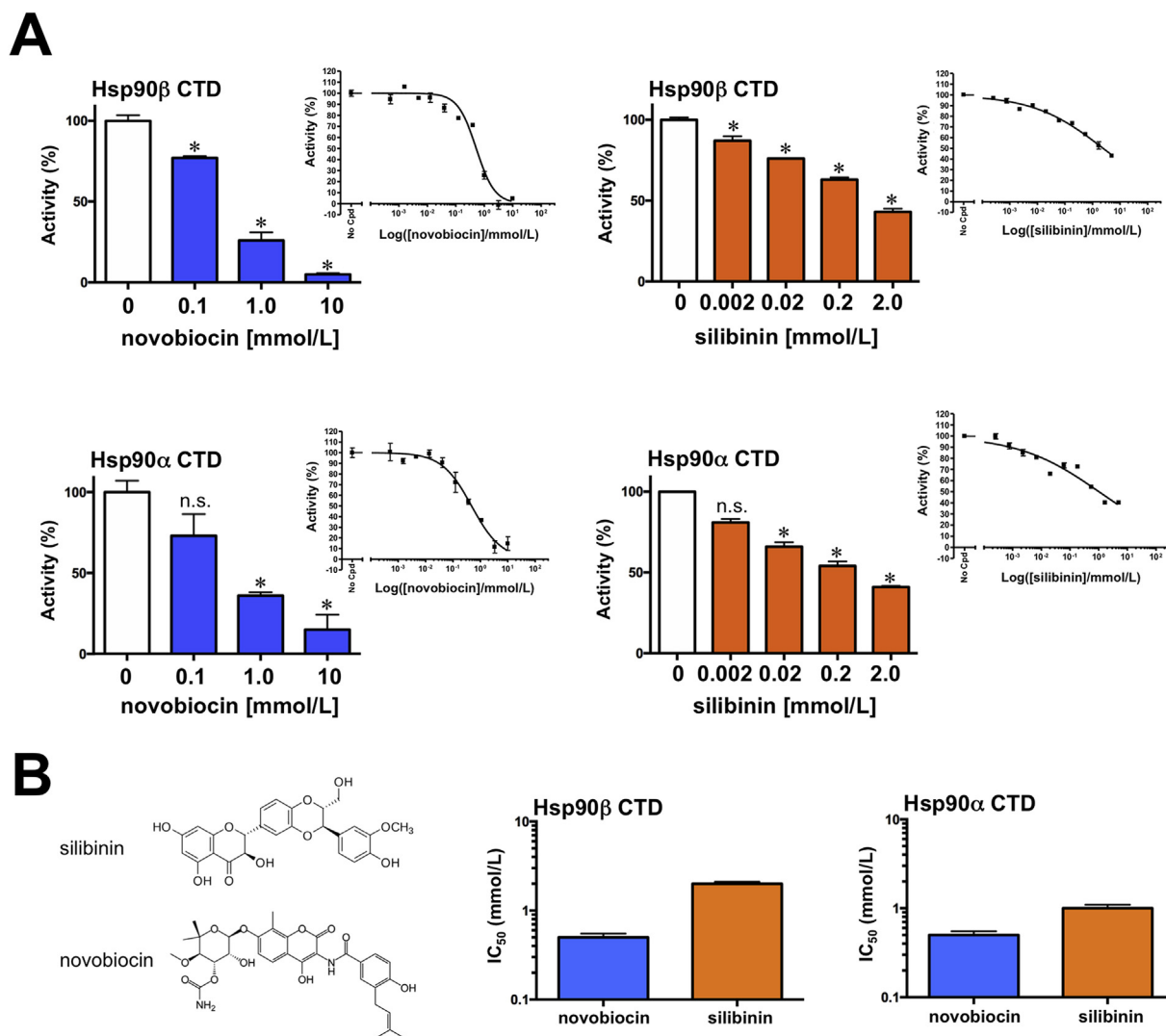
**Table 4**
Interactions between novobiocin/silibinin and the open conformation of the Hsp90α dimer.

| Cluster number | ΔG, [kcal/mol] | Dissoc. constant, [μM] | Participating amino acids interacting with novobiocin |
|---|---|---|---|
| 1 | −9.742 | 0.072280 | SER50, ASN51, SER53, ASP54, ASP57, ARG60, VAL136, GLN212, PHE213, ILE214, GLY215, TYR216, ASN291, LYS292, THR293, LYS294, PRO295, ILE296, TRP297, PHE312, SER315, LEU316, ASN318, LYS362, TYR364, ARG367, PHE369 (chain 1) |
| 2 | −9.375 | 0.134286 | ASN83, GLN85, ASP86, GLU200, GLU223, ASP240, LYS241, ASP264, GLU266, LYS270, ASP271, GLY272, LYS274, LYS275, LYS278, LYS279, ILE280, LYS283 (chain 2) |
| 3 | −9.311 | 0.149605 | ALA347, PRO348, PHE349, PHE352, ASN383, PHE384, PHE441, LYS443, ASN444, LEU447, PRO524, ILE525, ARG612, ILE613, ALA616, GLN617 (chain 1) and ALA616, LEU619, ARG620 (chain 2) |
| 4 | −9.012 | 0.247808 | GLU497, ARG612, LYS615, ALA616, LEU619, SER677 (chain 1) and GLU497, GLU611, ARG612, LYS615, ALA616, LEU619, MET625, ALA629, ALA630, PHE676, SER677, LEU678, GLU679 (chain 2) |

| Cluster number | ΔG, [kcal/mol] | Dissoc. constant, [μM] | Participating amino acids interacting with silibinin |
|---|---|---|---|
| 1 | −10.344 | 0.026166 | ARG46, ILE49, SER50, SER53, ASP54, ASP57, LYS209, HIS210, SER211, GLN212, PHE213, ILE214, GLY215, TRP297, GLU311, PHE312, SER315, LEU316, TRP320, LYS362, TYR364, VAL388 (chain 2) |
| 2 | −9.03 | 0.240393 | ALA347, PRO348, PHE349, PHE352, LYS356, LYS357, LYS358, ASN359, ASN360, GLU375, ASN383, PHE384, GLN440, PHE441, LYS443, ASN444 (chain 1) and ASP621, ASN622, SER623 (chain 2) |
| 3 | −8.902 | 0.298364 | GLU497, ARG612, LEU672, GLY675, PHE676, SER677, LEU678, PRO681 (chain 1) and ILE494, THR495, GLY496, GLU497, GLN501, VAL502, SER505, ALA608, ASN609, ARG612, LEU672, GLY675, SER677, LEU678, PRO681 (chain 2) |

excess silibinin and novobiocin were found to displace bound Hsp90α CTD in solution (Riebold et al., 2015a,b). Because both inhibitors induced chemical shift perturbations for a number of nuclear magnetic resonance (NMR) spectroscopy-detected amide signals, whereas only a few NMR signals were perturbed by either silibinin or novobiocin, it was proposed that both compounds should bind directly Hsp90α CTD in a similar region (Riebold et al., 2015a,b). Since then, however, no further understanding has been gained towards silibinin's mode of Hsp90 inhibition, either through interaction with the N-terminus, the C-terminus, or an alternative mode of action.
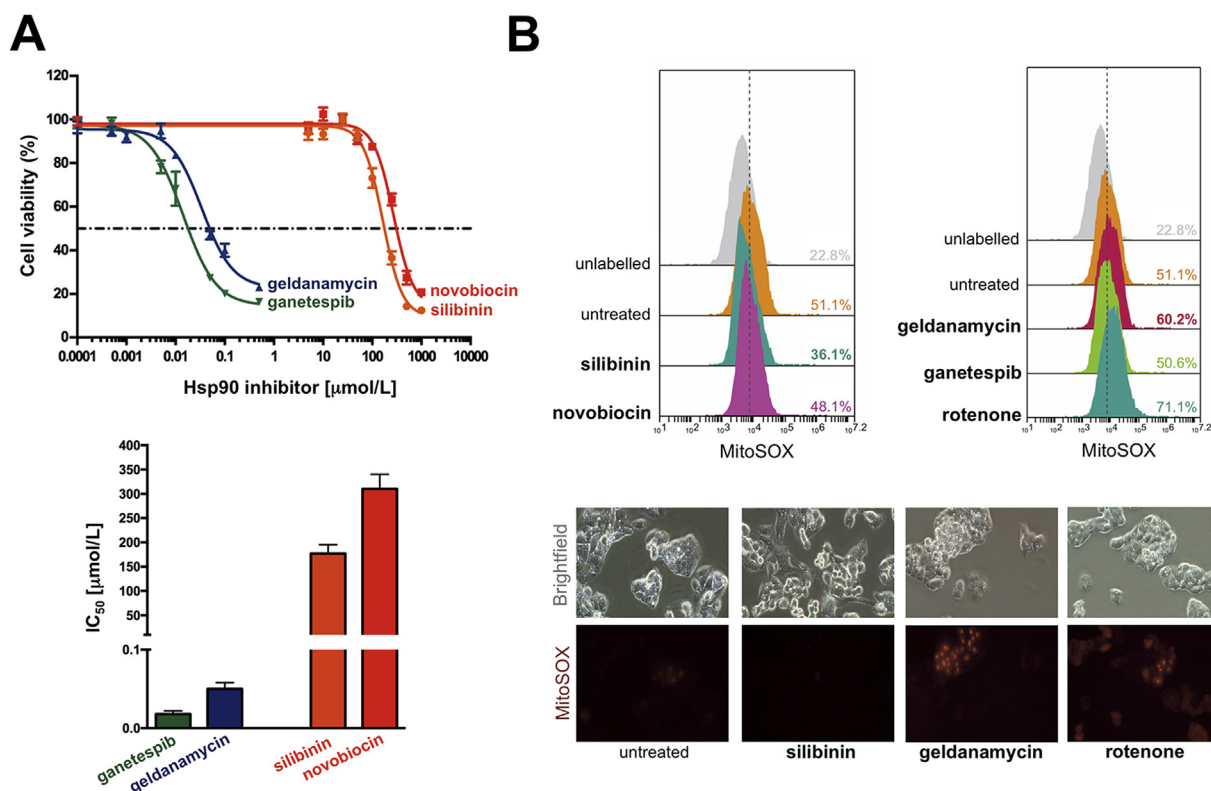
**Fig. 5. Novobiocin and silibinin effects on Hsp90α/β CTD activity. A.** The results of the effects of novobiocin and silibinin on Hsp90 CTD-PPID interaction are expressed as means (*columns*) ± SD (*bars*); two experimental replicates (*P < 0.05, statistically significant differences from the untreated (control) group; n.s. not statistically significant). **B.** The IC$_{50}$ values were calculated from sigmoidal dose-response curves shown as inserts in **A**.

Here, we performed a first-in-class computational study aimed at disentangling the putative molecular interactions between silibinin and Hsp90α/β by exploiting existing structures such as the atomic cryoEM structure of the Hsp90-Cdc37-Cdk4 complex (5FWM, Verba et al., 2016) or, alternatively, by generating computational homology models. Hsp90 has two isoforms in the cytoplasm. Hsp90β is expressed constitutively to a high level in most tissues and is generally more abundant than Hsp90α. By contrast, Hsp90α is stress-inducible and overexpressed in many tumor cells (Csermely et al., 1998; Chen et al., 2005; Millson et al., 2007), suggesting that it may be more closely involved in disease processes. The two Hsp90 isoforms share some common functions, but they possess distinct characteristics: Hsp90α is primarily involved in signal transduction, growth, and development (Voss et al., 2000), whereas Hsp90β plays a role in the heat-shock response (Millson et al., 2007). Hsp90 is known to recognize structure elements of a protein, thereby allowing other co-chaperones with enzymatic activity such as protein phosphatases and cis/trans peptidyl-prolyl isomerases (PPIase activity) to fold and repair the Hsp90-bound client (Karagöz et al., 2014). One of the co-chaperones with PPIase activity is the tetratricopeptide domain-containing peptidyl-prolyl isomerase D (PPID)/cyclophilin 40 (Cyp40). Our approach reveals that, whereas silibinin is predicted to interact with several pockets in the C-terminus of Hsp90α and β, its highest-ranking docked poses significantly overlap with those

of the well-characterized Hsp90 CTD-targeted inhibitor novobiocin. To date, however, only computational hypotheses have been proposed regarding the precise physical location and physiological role of the silibinin-binding site at the CTD of Hsp90 (Roy and Kapoor, 2016; Terracciano et al., 2018). Hsp90 is a very large protein with numerous conformation states, most of them lacking high-resolution structures. Moreover, while exerting its catalytic function, Hsp90 experiences great rearrangements in its secondary, tertiary, and quaternary structure. All of these features make it challenging to rationally explain the binding mode of silibinin, which has been described here solely for the open and closed states, but not for any of the multiple intermediate conformations of Hsp90α/β. Nonetheless, because the Hsp90-binding site of novobiocin involves a region of the CTD dimerization domain of the chaperone (Marcu et al., 2000a,b), it is tempting to speculate that silibinin may antagonize Hsp90 function by inducing a conformation favoring separation of the CTDs and release of substrate (Allan et al., 2006). Indeed, the currently predicted binding sites for both silibinin and novobiocin favorably locate in the broad C-terminal region of Hsp90, in many cases at the interface between the subunits making up the Hsp90 dimer. Given the high energies reported for the binding of silibinin to novobiocin-like locations at the CTD of Hsp90, it is reasonable to suggest that silibinin would impair the structural rearrangements necessary for Hsp90 functioning, perhaps involving

**Fig. 6. Hepatotoxic and superoxide-producing effects of Hsp90 inhibitors. A.** Dose-response curves obtained by MTT assays for HepG2 cells exposed to Hsp90 inhibitors. Plotted is the percentage of cell viability (y-axis) through exposure to geldanamycin, ganetespib (STA-909), novobiocin, and silibinin at increasing doses (x-axis). The results are expressed as means ± SD of three experimental replicates. The IC$_{50}$ values were determined as the concentration causing a half-maximal percent cytotoxic activity. **B.** Histograms showing MitoSOX reactive ROS levels in HepG2 cells following 18 h treatment with 50 nmol/L geldanamycin, 50 nmol/L ganetespib (STA-909), 250 μmol/L novobiocin, 250 μmol/L silibinin, and 2 μmol/L rotenone. Inserts show fluorescence microphotographs demonstrating representative MitoSOX-reactive ROS (red) in HepG2 cells with the treatment conditions mentioned above. (For interpretation of the references to color in this figure legend, the reader is referred to the Web version of this article.)

competitive phenomena at the CTD ATP-binding site. The computational predictions of additional, numerous high-affinity binding sites in the middle domain of Hsp90 further suggest the ability of silibinin to disrupt the Hsp90-co-chaperone-client interactions. Accordingly, the net biochemical effect of silibinin was to inhibit the efficiency of the Hsp90α/β CTD binding to its co-chaperone PPID/cyclophilin D in a low millimolar range equivalent to that observed with novobiocin (Yun et al., 2004a,b).

The most clinically significant off-target, Hsp90-independent toxicity observed with the first-generation of geldanamycin-based inhibitors was dose-limiting hepatotoxicity (Nowakowski et al., 2006; Solit et al., 2007). Such impairment of liver function likely reflects the P450-associated redox active properties of the benzoquinone moiety of geldanamycin and the extent of geldanamycin-driven superoxide formation, which may stimulate hepatocytes oxidative injury (Samuni et al., 2010). Our findings support the notion that silibinin, which does not influence the activities of major P450 drug-metabolizing enzymes and is well tolerated *in vivo* (Kawaguchi-Suzuki et al., 2014; Soleimani et al., 2019), might provide an advantageous toxicological profile as a non-quinone Hsp90 inhibitor capable of decreasing hepatic ROS levels (Detaille et al., 2008; Serviddio et al., 2014). Moreover, next-generation Hsp90 inhibitors such ganetespib lacking the dose-limiting hepatotoxicity reported with the geldanamycin analogs (Wang et al., 2010; Shimamura et al., 2012; Jhaveri and Modi, 2015) are mostly aimed to block the binding of ATP to the N-terminus of Hsp90, a mechanism of action that activates a cytoprotective resistance response called heat shock response (HSR). Using HepG2 cells, a predictive model of hepatoxicants in which the Hsp90 inhibition-related endoplasmic reticulum stress and unfolded protein responses (Marcu et al., 2002; Davenport

et al., 2007; Graner et al., 2017) are the main cellular effects underlying drug-induced liver injury (Van den Hof et al., 2014), we indirectly provide evidence that the client depletion activity of silibinin as a novobiocin-like C-terminal inhibitor of Hsp90 is not expected to trigger such undesirable HSR involving a large increase in several prosurvival proteins (Koay et al., 2016; Bhatia et al., 2018). Such triggering of less off-target effects by silibinin is supported by the notably lower difference between its inhibitory concentration required to block purified Hsp90 protein activity in biochemical assays (1–2 mmol/L) and its cytotoxic activity against cultured cancer cells (typically ranging from 50 to 150 μmol/L; Bosch-Barrera et al., 2017), a difference that might reach > 100-fold in the case of N-terminal-targeted Hsp90 inhibitors (Wang and McAlpine, 2015).

Our computational-experimental approach unequivocally confirms that silibinin might be viewed as a novobiocin-like Hsp90 inhibitor that binds the CTD of Hsp90 to induce changes in its conformation, and alter Hsp90-co-chaperone-client interactions (Zhao et al., 2011; Riebold et al., 2015a,b). Given the essential role of Hsp90 for the functional competence of STAT3 activity governing tumor microenvironment and metastatic progression (Bocchini et al., 2014; Cho et al., 2019), and the recently proposed model of stress-inducible expression of Hsp90β after the transition of quiescent astrocytes to the reactive phenotype (Sha et al., 2017), our current findings provide a new framework in which the non-mutually exclusive direct effects of silibinin on STAT3 and Hsp90 may explain its unexpected clinical activity in the molecular dialogue between metastatic cancer cells and the brain microenvironment.

## 5. Conclusions

Our computational findings coupled to experimental validation, together with the capacity of silibinin structure to avoid unwanted biotransformation phenomena responsible for hepatotoxicity and its lack of adverse effects even when employed at high doses, strongly suggest that the novobiocin-like behavior of silibinin as an Hsp90 CTD inhibitor might represent a new promising path to develop safe and efficacious Hsp90 inhibitors for cancer therapy.

## Declaration of interests

The authors declare that they have no known competing financial interests or personal relationships that could have appeared to influence the work reported in this paper.

## Acknowledgments

## Appendix A. Supplementary data

Supplementary data to this article can be found online at https://doi.org/10.1016/j.fct.2019.110645.

## Transparency document

Transparency document related to this article can be found online at https://doi.org/10.1016/j.fct.2019.110645

## References

Abenavoli, L., Izzo, A.A., Milić, N., Cicala, C., Santini, A., Capasso, R., 2018. Milk thistle (Silybum marianum): a concise overview on its chemistry, pharmacological, and nutraceutical uses in liver diseases. Phytother Res. 32, 2202–2213.

Agarwal, C., Tyagi, A., Kaur, M., Agarwal, R., 2007. Silibinin inhibits constitutive activation of Stat3, and causes caspase activation and apoptotic death of human prostate carcinoma DU145 cells. Carcinogenesis 28, 1463–1470.

Allan, R.K., Mok, D., Ward, B.K., Ratajczak, T., 2006. Modulation of chaperone function and cochaperone interaction by novobiocin in the C-terminal domain of Hsp90: evidence that coumarin antibiotics disrupt Hsp90 dimerization. J. Biol. Chem. 281, 7161–7171.

Barrott, J.J., Haystead, T.A., 2013. Hsp90, an unlikely ally in the war on cancer. FEBS J. 280, 1381–1396.

Bello-Pérez, M., Falcó, A., Galiano, V., Coll, J., Perez, L., Encinar, J.A., 2018. Discovery of nonnucleoside inhibitors of polymerase from infectious pancreatic necrosis virus (IPNV). Drug Des. Dev. Ther. 12, 2337–2359.

Bhatia, S., Diedrich, D., Frieg, B., Ahlert, H., Stein, S., Bopp, B., Lang, F., Zang, T., Kröger, T., Ernst, T., Kögler, G., Krieg, A., Lüdeke, S., Kunkel, H., Rodrigues Moita, A.J., Kassack, M.U., Marquardt, V., Opitz, F.V., Oldenburg, M., Remke, M., Babor, F., Grez, M., Hochhaus, A., Borkhardt, A., Groth, G., Nagel-Steger, L., Jose, J., Kurz, T., Gohlke, H., Hansen, F.K., Hauer, J., 2018. Targeting HSP90 dimerization via the C terminus is effective in imatinib-resistant CML and lacks the heat shock response. Blood 132, 307–320.

Biasini, M., Bienert, S., Waterhouse, A., Arnold, K., Studer, G., Schmidt, T., Kiefer, F., Gallo Cassarino, T., Bertoni, M., Bordoli, L., Schwede, T., 2014. SWISS-MODEL: modelling protein tertiary and quaternary structure using evolutionaryinformation. Nucleic Acids Res. 42 (Web Server issue), W252–W258.

Blair, L.J., Sabbagh, J.J., Dickey, C.A., 2014. Targeting Hsp90 and its co-chaperones to treat Alzheimer's disease. Expert Opin. Ther. Targets 18, 1219–1232.

Bocchini, C.E., Kasembeli, M.M., Roh, S.H., Tweardy, D.J., 2014. Contribution of chaperones to STAT pathway signaling. JAK-STAT 3, e970459.

Bosch-Barrera, J., Menendez, J.A., 2015. Silibinin and STAT3: a natural way of targeting transcription factors for cancer therapy. Cancer Treat Rev. 41, 540–546.

Bosch-Barrera, J., Corominas-Faja, B., Cuyàs, E., Martin-Castillo, B., Brunet, J., Menendez, J.A., 2014. Silibinin administration improves hepatic failure due to extensive liver infiltration in a breast cancer patient. Anticancer Res. 34, 4323–4327.

Bosch-Barrera, J., Sais, E., Cañete, N., Marruecos, J., Cuyàs, E., Izquierdo, A., Porta, R., Haro, M., Brunet, J., Pedraza, S., Menendez, J.A., 2016. Response of brain metastasis from lung cancer patients to an oral nutraceutical product containing silibinin. Oncotarget 7, 32006–32014.

Bosch-Barrera, J., Queralt, B., Menendez, J.A., 2017. Targeting STAT3 with silibinin to improve cancer therapeutics. Cancer Treat Rev. 58, 61–69.

Chatterjee, S., Burns, T.F., 2017. Targeting heat shock proteins in cancer: a promising therapeutic approach. Int. J. Mol. Sci. 18 (9) pii: E1978.

Chen, B., Piel, W.H., Gui, L., Bruford, E., Monteiro, A., 2005. The HSP90 family of genes in the human genome: insights into their divergence and evolution. Genomics 86, 627–637.

Cho T-M, Kim JY, Kim Y-J, Sung D, Oh E, Jang S, Farrand L, Hoang V-H, Nguyen C-T, Ann J, Lee J, Seo JH. C-terminal hsp90 inhibitor L80 elicits anti-metastatic effects in triple-negative breast cancer via STAT3 inhibiton. Cancer Lett., https://doi.org/10.1016/j.canlet.2019.01.029.

Csermely, P., Schnaider, T., Soti, C., Prohászka, Z., Nardai, G., 1998. The 90-kDa molecular chaperone family: structure, function, and clinical applications. A comprehensive review. Pharmacol. Ther. 79, 129–168.

Cuyàs, E., Pérez-Sánchez, A., Micol, V., Menendez, J.A., Bosch-Barrera, J., 2016. STAT3-targeted treatment with silibinin overcomes the acquired resistance to crizotinib in ALK-rearranged lung cancer. Cell Cycle 15, 3413–3418.

Cysyk, R.L., Parker, R.J., Barchi Jr., J.J., Steeg, P.S., Hartman, N.R., Strong, J.M., 2006. Reaction of geldanamycin and C17-substituted analogues with glutathione: product identifications and pharmacological implications. Chem. Res. Toxicol. 19, 376–381.

Davenport, E.L., Moore, H.E., Dunlop, A.S., Sharp, S.Y., Workman, P., Morgan, G.J., Davies, F.E., 2007. Heat shock protein inhibition is associated with activation of the unfolded protein responsepathway in myeloma plasma cells. Blood 110, 2641–2649.

Detaille, D., Sanchez, C., Sanz, N., Lopez-Novoa, J.M., Leverve, X., El-Mir, M.Y., 2008. Interrelation between the inhibition of glycolytic flux by silibinin and the lowering of mitochondrial ROS production in perifused rat hepatocytes. Life Sci. 82, 1070–1076.

Dikalov, S., Landmesser, U., Harrison, D.G., 2002. Geldanamycin leads to superoxide formation by enzymatic and non-enzymatic redox cycling. Implications for studies of Hsp90 and endothelial cell nitric-oxidase synthase. J. Biol. Chem. 277, 25480–25485.

Dollins, D.E., Warren, J.J., Immormino, R.M., Gewirth, D.T., 2007. Structures of GRP94-nucleotide complexes reveal mechanistic differences between the hsp90 chaperones. Mol. Cell 28, 41–56.

Egorin, M.J., Rosen, D.M., Wolff, J.H., Callery, P.S., Musser, S.M., Eiseman, J.L., 1998. Metabolism of 17-(allylamino)-17-demethoxygeldanamycin (NSC 330507) by murine and human hepatic preparations. Cancer Res. 58, 2385–2396.

Encinar, J.A., Fernández-Ballester, G., Galiano-Ibarra, V., Micol, V., 2015. In silico approach for the discovery of new PPARγ modulators among plant-derived polyphenols. Drug Des. Dev. Ther. 9, 5877–5895.

Federico, A., Dallio, M., Loguercio, C., 2017. Silymarin/Silybin and chronic liver disease: a marriage of many years. Molecules 22 (2) pii: E191.

Galiano, V., Garcia-Valtanen, P., Micol, V., Encinar, J.A., 2016. Looking for inhibitors of the dengue virus NS5 RNA-dependent RNA-polymerase using a molecular docking approach. Drug Des. Dev. Ther. 10, 3163–3181.

Gallegos Ruiz, M.I., Floor, K., Roepman, P., Rodriguez, J.A., Meijer, G.A., Mooi, W.J., Jassem, E., Niklinski, J., Muley, T., van Zandwijk, N., Smit, E.F., Beebe, K., Neckers, L., Ylstra, B., Giaccone, G., 2008. Integration of gene dosage and gene expression in non-small cell lung cancer, identification of HSP90 as potential target. PLoS One 3, e0001722.

Gazák, R., Walterová, D., Kren, V., 2007. Silybin and silymarin–new and emerging applications in medicine. Curr. Med. Chem. 14, 315–338.

Graner, A.N., Hellwinkel, J.E., Lencioni, A.M., Madsen, H.J., Harland, T.A., Marchando, P., Nguyen, G.J., Wang, M., Russell, L.M., Bemis, L.T., Anchordoquy, T.J., Graner, M.W., 2017. HSP90 inhibitors in the context of heat shock and the unfolded protein response: effects on a primary canine pulmonary adenocarcinoma cell line. Int. J. Hyperth. 33, 303–317.

Hadden, M.K., Galam, L., Gestwicki, J.E., Matts, R.L., Blagg, B.S., 2007. Derrubone, an inhibitor of the Hsp90 protein folding machinery. J Nat Prod 70, 2014–2018.

Hastings, J.M., Hadden, M.K., Blagg, B.S., 2008. Synthesis and evaluation of derrubone and select analogues. J. Org. Chem. 73, 369–373.

Jahanafrooz, Z., Motamed, N., Rinner, B., Mokhtarzadeh, A., Baradaran, B., 2018 Nov 15. Silibinin to improve cancer therapeutic, as an apoptotic inducer, autophagy modulator, cell cycle inhibitor, and microRNAs regulator. Life Sci. 213, 236–247.

Jhaveri, K., Modi, S., 2015. Ganetespib: research and clinical development. OncoTargets Ther. 8, 1849–1858.

Karagöz, G.E., Duarte, A.M., Akoury, E., Ippel, H., Biernat, J., Morán Luengo, T., Radli, M., Didenko, T., Nordhues, B.A., Veprintsev, D.B., Dickey, C.A., Mandelkow, E., Zweckstetter, M., Boelens, R., Madl, T., Rüdiger, S.G., 2014. Hsp90-Tau complex reveals molecular basis for specificity in chaperone action. Cell. 156, 963–974.

Kawaguchi-Suzuki, M., Frye, R.F., Zhu, H.J., Brinda, B.J., Chavin, K.D., Bernstein, H.J., Markowitz, J.S., 2014. The effects of milk thistle (Silybum marianum) on human cytochrome P450 activity. Drug Metab. Dispos. 42, 1611–1616.

Koay, Y.C., Wahyudi, H., McAlpine, S.R., 2016. Reinventing Hsp90 inhibitors: blocking C-

terminal binding events by Hsp90 using dimerized inhibitors. Chemistry 22, 18572–18582.

Krieger, E., Vriend, G., 2014. YASARA View - molecular graphics for all devices - from smartphones to workstations. Bioinformatics 30, 2981–2982.

Krieger, E., Darden, T., Nabuurs, S.B., Finkelstein, A., Vriend, G., 2004. Making optimal use of empirical energy functions: force-field parameterization in crystal space. Proteins 57, 678–683.

Lauber, K., Brix, N., Ernst, A., Hennel, R., Krombach, J., Anders, H., Belka, C., 2015. Targeting the heat shock response in combination with radiotherapy: sensitizing cancer cells to irradiation-induced cell death and heating up their immunogenicity. Cancer Lett. 368, 209–229.

Lionta, E., Spyrou, G., Vassilatis, D.K., Cournia, Z., 2014. Structure-based virtual screening for drug discovery: principles, applications and recent advances. Curr. Top. Med. Chem. 14, 1923–1938.

Marcu, M.G., Chadli, A., Bouhouche, I., Catelli, M., Neckers, L.M., 2000a. The heat shock protein 90 antagonist novobiocin interacts with a previously unrecognized ATP-binding domain in the carboxyl terminus of the chaperone. J. Biol. Chem. 275, 37181–37186.

Marcu, M.G., Schulte, T.W., Neckers, L., 2000b. Novobiocin and related coumarins and depletion of heat shock protein 90-dependent signaling proteins. J Natl Cancer Inst 92, 242–248.

Marcu, M.G., Doyle, M., Bertolotti, A., Ron, D., Hendershot, L., Neckers, L., 2002. Heat shock protein 90 modulates the unfolded protein response by stabilizing IRE1alpha. Mol. Cell. Biol. 22, 8506–8513.

Mateen, S., Raina, K., Agarwal, R., 2013. Chemopreventive and anti-cancer efficacy of silibinin against growth and progression of lung cancer. Nutr. Canc. 65 (Suppl. 1), 3–11.

Matts, R.L., Dixit, A., Peterson, L.B., Sun, L., Voruganti, S., Kalyanaraman, P., Hartson, S.D., Verkhivker, G.M., Blagg, B.S., 2011. Elucidation of the Hsp90 C-terminal inhibitor binding site. ACS Chem. Biol. 6, 800–807.

Mays, J.R., Hill, S.A., Moyers, J.T., Blagg, B.S., 2010. The synthesis and evaluation of flavone and isoflavone chimeras of novobiocin and derrubone. Bioorg. Med. Chem. 18, 249–266.

Millson, S.H., Truman, A.W., Rácz, A., Hu, B., Panaretou, B., Nuttall, J., Mollapour, M., Söti, C., Piper, P.W., 2007. Expressed as the sole Hsp90 of yeast, the alpha and beta isoforms of human Hsp90 differ with regard to their capacities for activation of certain client proteins, whereas only Hsp90betagenerates sensitivity to the Hsp90 inhibitor radicicol. FEBS J. 274, 4453–4463.

Neckers, L., Workman, P., 2012. Hsp90 molecular chaperone inhibitors: are we there yet? Clin. Cancer Res. 18, 64–76.

Nowakowski, G.S., McCollum, A.K., Ames, M.M., Mandrekar, S.J., Reid, J.M., Adjei, A.A., Toft, D.O., Safgren, S.L., Erlichman, C., 2006. A phase I trial of twice-weekly 17-allylamino-demethoxy-geldanamycin in patients with advanced cancer. Clin. Cancer Res. 12, 6087–6093.

Pérez-Sánchez, A., Cuyàs, E., Ruiz-Torres, V., Agulló-Chazarra, L., Verdura, S., González-Álvarez, I., Bermejo, M., Joven, J., Micol, V., Bosch-Barrera, J., Menendez, J.A., 2019. Intestinal permeability study of clinically relevant formulations of silibinin in caco-2 cell monolayers. Int. J. Mol. Sci. 20 pii: E1606.

Priego, N., Zhu, L., Monteiro, C., Mulders, M., Wasilewski, D., Bindeman, W., Doglio, L., Martínez, L., Martínez-Saez, E., Cajal, S.R.Y., Megías, D., Hernández-Encinas, E., Blanco-Aparicio, C., Martínez, L., Zarzuela, E., Muñoz, J., Fustero-Torre, C., Piñeiro-Yáñez, E., Hernández-Laín, A., Bertero, L., Poli, V., Sanchez-Martinez, M., Menendez, J.A., Soffietti, R., Bosch-Barrera, J., Valiente, M., 2018. STAT3 labels a subpopulation of reactive astrocytes required for brain metastasis. Nat. Med. 24, 1024–1035.

Ramirez, T., Strigun, A., Verlohner, A., Huener, H.A., Peter, E., Herold, M., Bordag, N., Mellert, W., Walk, T., Spitzer, M., Jiang, X., Sperber, S., Hofmann, T., Hartung, T., Kamp, H., van Ravenzwaay, B., 2018. Prediction of liver toxicity and mode of action using metabolomics in vitro in HepG2 cells. Arch. Toxicol. 92, 893–906.

Riebold, M., Kozany, C., Freiburger, L., Sattler, M., Buchfelder, M., Hausch, F., Stalla, G.K., Paez-Pereda, M., 2015a. A C-terminal HSP90 inhibitor restores glucocorticoid sensitivity and relieves a mouse allograft model of Cushing disease. Nat. Med. 21, 276–280.

Riebold, M., Kozany, C., Freiburger, L., Sattler, M., Buchfelder, M., Hausch, F., Stalla, G.K., Paez-Pereda, M., 2015b. A C-terminal HSP90 inhibitor restores glucocorticoid sensitivity and relieves a mouse allograft model of Cushing disease. Nat. Med. 21, 276–280.

Roy, S.S., Kapoor, M., 2016. In silico identification and computational analysis of the nucleotide binding site in the C-terminaldomain of Hsp90. J. Mol. Graph. Model. 70, 253–274.

Salentin, S., Schreiber, S., Haupt, V.J., Adasme, M.F., Schroeder, M., 2015. PLIP: fully automated protein-ligand interaction profiler. Nucleic Acids Res. 43, W443–W447.

Samuni, Y., Ishii, H., Hyodo, F., Samuni, U., Krishna, M.C., Goldstein, S., Mitchell, J.B., 2010. Reactive oxygen species mediate hepatotoxicity induced by the Hsp90 inhibitor geldanamycin and its analogs. Free Radic. Biol. Med. 48, 1559–1563.

Sbiera, S., Deutschbein, T., Weigand, I., Reincke, M., Fassnacht, M., Allolio, B., 2015. The new molecular landscape of cushing's disease. Trends Endocrinol Metab 26, 573–583.

Schymkowitz, J., Borg, J., Stricher, F., Nys, R., Rousseau, F., Serrano, L., 2005. The FoldX web server: an online force field. Nucleic Acids Res. 33, W382–W388 (Web Server issue).

Sequist, L.V., Gettinger, S., Senzer, N.N., Martins, R.G., Jänne, P.A., Lilenbaum, R., Gray, J.E., Iafrate, A.J., Katayama, R., Hafeez, N., Sweeney, J., Walker, J.R., Fritz, C., Ross, R.W., Grayzel, D., Engelman, J.A., Borger, D.R., Paez, G., Natale, R., 2010. Activity of IPI-504, a novel heat-shock protein 90 inhibitor, in patients with molecularly defined non-small-cell lung cancer. J. Clin. Oncol. 28, 4953–4960.

Servddio, G., Bellanti, F., Stanca, E., Lunetti, P., Blonda, M., Tamborra, R., Siculella, L., Vendemiale, G., Capobianco, L., Giudetti, A.M., 2014. Silybin exerts antioxidant effects and induces mitochondrial biogenesis in liver of rat with secondary biliary

cirrhosis. Free Radic. Biol. Med. 73, 117–126.

Sha, L., Wang, X., Li, J., Shi, X., Wu, L., Shen, Y., Xu, Q., 2017. Pharmacologic inhibition of Hsp90 to prevent GLT-1 degradation as an effective therapy for epilepsy. J. Exp. Med. 214, 547–563.

Shao, J., Grammatikakis, N., Scroggins, B.T., Uma, S., Huang, W., Chen, J.J., Hartson, S.D., Matts, R.L., 2001. Hsp90 regulates p50(cdc37) function during the biogenesis of the activeconformation of the heme-regulated eIF2 alpha kinase. J. Biol. Chem. 276, 206–214.

Shao, J., Irwin, A., Hartson, S.D., Matts, R.L., 2003. Functional dissection of cdc37: characterization of domain structure and amino acid residues critical for protein kinase binding. Biochemistry 42, 12577–12588.

Shimamura, T., Perera, S.A., Foley, K.P., Sang, J., Rodig, S.J., Inoue, T., Chen, L., Li, D., Carretero, J., Li, Y.C., Sinha, P., Carey, C.D., Borgman, C.L., Jimenez, J.P., Meyerson, M., Ying, W., Barsoum, J., Wong, K.K., Shapiro, G.I., 2012. Ganetespib (STA-9090), a nongeldanamycin HSP90 inhibitor, has potent antitumor activity in in vitro and in vivo models of non-small cell lung cancer. Clin. Cancer Res. 18, 4973–4985.

Shimura, T., Sasatani, M., Kawai, H., Kamiya, K., Kobayashi, J., Komatsu, K., Kunugita, N., 2017. ATM-mediated mitochondrial damage response triggered by nuclear DNA damage in normal human lung fibroblasts. Cell Cycle 16, 2345–2354.

Socinski, M.A., Goldman, J., El-Hariry, I., Koczywas, M., Vukovic, V., Horn, L., Paschold, E., Salgia, R., West, H., Sequist, L.V., Bonomi, P., Brahmer, J., Chen, L.C., Sandler, A., Belani, C.P., Webb, T., Harper, H., Huberman, M., Ramalingam, S., Wong, K.K., Teofilovici, F., Guo, W., Shapiro, G.I., 2013. A multicenter phase II study of gane-tespib monotherapy in patients with genotypically defined advanced non-small cell lung cancer. Clin. Cancer Res. 19, 3068–3077.

Soleimani, V., Delghandi, P.S., Moallem, S.A., Karimi, G., 2019. Safety and toxicity of silymarin, the major constituent of milk thistle extract: an updated review. Phytother Res. https://doi.org/10.1002/ptr.6361. ([Epub ahead of print]).

Solit, D.B., Ivy, S.P., Kopil, C., Sikorski, R., Morris, M.J., Slovin, S.F., Kelly, W.K., DeLaCruz, A., Curley, T., Heller, G., Larson, S., Schwartz, L., Egorin, M.J., Rosen, N., Scher, H.I., 2007. Phase I trial of 17-allylamino-17-demethoxygeldanamycin in patients with advanced cancer. Clin. Cancer Res. 13, 1775–1782.

Sugiyama, A., Kageyama, K., Murasawa, S., Ishigame, N., Niioka, K., Daimon, M., 2015. Inhibition of heat shock protein 90 decreases ACTH production and cell proliferation in AtT-20 cells. Pituitary 18, 542–553.

Taherian, A., Krone, P.H., Ovsenek, N., 2008. A comparison of Hsp90alpha and Hsp90beta interactions with cochaperones and substrates. Biochem. Cell Biol. 86, 37–45.

Terracciano, S., Russo, A., Chini, M.G., Vaccaro, M.C., Potenza, M., Vassallo, A., Riccio, R., Bifulco, G., Bruno, I., 2018. Discovery of new molecular entities able to strongly interfere with Hsp90 C-terminal domain. Sci. Rep. 8, 1709.

Thulasiraman, V., Matts, R.L., 1996. Effect of geldanamycin on the kinetics of chaperone-mediated renaturation of firefly luciferase in rabbit reticulocyte lysate. Biochemistry 35, 13443–13450.

Tiwari, P., Mishra, K.P., 2015. Silibinin in cancer therapy: a promising prospect. Cancer Res Front 1, 303–318.

Travers, J., Sharp, S., Workman, P., 2012. HSP90 inhibition: two-pronged exploitation of cancer dependencies. Drug Discov. Today 17, 242–252.

Uma, S., Hartson, S.D., Chen, J.J., Matts, R.L., 1997. Hsp90 is obligatory for the heme-regulated eIF-2alpha kinase to acquire and maintain an activable conformation. J. Biol. Chem. 272, 11648–11656.

Van den Hof, W.F., Coonen, M.L., van Herwijnen, M., Brauers, K., Wodzig, W.K., van Delft, J.H., Kleinjans, J.C., 2014. Classification of hepatotoxicants using HepG2 cells: a proof of principle study. Chem. Res. Toxicol. 27, 433–442.

Vargas-Mendoza, N., Madrigal-Santillán, E., Morales-González, A., Esquivel-Soto, J., Esquivel-Chirino, C., García-Luna Y González-Rubio, M., Gayosso-de-Lucio, J.A., Morales-González, J.A., 2014. Hepatoprotective effect of silymarin. World J. Hepatol. 6, 144–149.

Verba, K.A., Wang, R.Y., Arakawa, A., Liu, Y., Shirouzu, M., Yokoyama, S., Agard, D.A., 2016. Atomic structure of Hsp90-Cdc37-Cdk4 reveals that Hsp90 traps and stabilizes an unfolded kinase. Science 352, 1542–1547.

Verdura, S., Cuyàs, E., Llorach-Parés, L., Pérez-Sánchez, A., Micol, V., Nonell-Canals, A., Joven, J., Valiente, M., Sánchez-Martínez, M., Bosch-Barrera, J., Menendez, J.A., 2018. Silibinin is a direct inhibitor of STAT3. Food Chem. Toxicol. 116, 161–172.

Voss, A.K., Thomas, T., Gruss, P., 2000. Mice lacking HSP90beta fail to develop a pla-cental labyrinth. Development 127, 1–11.

Wang, Y., McAlpine, S.R., 2015. N-terminal and C-terminal modulation of Hsp90 produce dissimilar phenotypes. Chem Commun (Camb) 51, 1410–1413.

Wang, Y., Trepel, J.B., Neckers, L.M., Giaccone, G., 2010. STA-9090, a small-molecule Hsp90 inhibitor for the potential treatment of cancer. Curr. Opin. Investig. Drugs 11, 1466–1476.

Young, J.C., Hoogenraad, N.J., Hartl, F.U., 2003. Molecular chaperones Hsp90 and Hsp70 deliver preproteins to the mitochondrial import receptor Tom70. Cell 112, 41–50.

Yun, B.G., Huang, W., Leach, N., Hartson, S.D., Matts, R.L., 2004a. Novobiocin induces a distinct conformation of Hsp90 and alters Hsp90-cochaperone-client interactions. Biochemistry 43, 8217–8229.

Yun, B.G., Huang, W., Leach, N., Hartson, S.D., Matts, R.L., 2004b. Novobiocin induces a distinct conformation of Hsp90 and alters Hsp90-cochaperone-client interactions. Biochemistry 43, 8217–8229.

Zhang, I., Zaorsky, N.G., Palmer, J.D., Mehra, R., Lu, B., 2015. Targeting brain metastases in ALK-rearranged non-small-cell lung cancer. Lancet Oncol. 16, e510–e521.

Zhao, H., Brandt, G.E., Galam, L., Matts, R.L., Blagg, B.S., 2011. Identification and initial SAR of silybin: an Hsp90 inhibitor. Bioorg. Med. Chem. Lett 21, 2659–2664.

Zhao, H., Yan, B., Peterson, L.B., Blagg, B.S., 2012. 3-Arylcoumarin derivatives manifest anti-proliferative activity through Hsp90 inhibition. ACS Med. Chem. Lett. 3, 327–331 Epub 2012 Feb 26.